APPLIED AND ENVIRONMENTAL MICROBIOLOGY, Apr. 2006, p. 3021–3025 Vol. 72, No. 4
0099-2240/06/$08.00+0 doi:10.1128/AEM.72.4.3021–3025.2006

Analysis of the Thermostability Determinants of Hyperthermophilic Esterase EstE1 Based on Its Predicted Three-Dimensional Structure

Jin-Kyu Rhee,[1] Do-Yun Kim,[2] Dae-Gyun Ahn,[1] Jung-Hyuk Yun,[2] Seung-Hwan Jang,[3] Hang-Cheol Shin,[3] Hyun-Soo Cho,[4] Jae-Gu Pan,[5] and Jong-Won Oh[1]*

Department of Biotechnology, Yonsei University, Seoul 120-749, South Korea[1]; R&D Center, IDRTech Inc., Sungnam 463-480, South Korea[2]; Department of Bioinformatics and Life Science and CAMDRC, Soongsil University, Seoul 156-743, South Korea[3]; Department of Biology, Yonsei University, Seoul 120-749, South Korea[4]; and Korea Research Institute of Bioscience and Biotechnology, Taejon 305-600, South Korea[5]

Received 22 December 2005/Accepted 6 February 2006

The three-dimensional (3D) structure of the hyperthermophilic esterase EstE1 was constructed by homology modeling using *Archaeoglobus fulgidus* esterase as a reference, and the thermostability-structure relationship was analyzed. Our results verified the predicted 3D structure of EstE1 and identified the ion pair networks and hydrophobic interactions that are critical determinants for the thermostability of EstE1.

We previously isolated the hyperthermophilic esterase EstE1 as a new thermophilic esterase belonging to the mammalian hormone-sensitive lipase (HSL) family by functional screening of a metagenomic library constructed with metagenomes from a thermal environment in Indonesia (17). In the HSL family esterase/lipase, three-dimensional (3D) structures have been reported for an esterase from the mesophilic bacterium *Alcaligenes eutrophus* (2), the brefeldin A esterase (BFAE) from the mesophilic bacterium *Bacillus subtilis* (20), and two thermostable esterases, EST2 from *Alicyclobacillus acido caldarius* (5) and AFEST from *Archaeoglobus fulgidus* (6). These HSL family esterases have equivalent functions, sequence homologies, and similar 3D structures (14). However, they have different thermostabilities. Therefore, comparison of their structures and sequences can help identify crucial factors for the thermostability of proteins. Lacking knowledge of the EstE1 3D structure, we used a combined approach of sequence comparison and molecular modeling to study the thermostability-structure relationship of EstE1.

First, we built a 3D model structure of EstE1 (NCBI accession number AY726780) by homology modeling using AFEST as a template, which has a 48.9% amino acid sequence identity to EstE1. The final model structure had 10 α-helices and 8 β-sheets (Fig. 1). The central β-sheet consisted of eight β strands (β1 to β8) with a left-handed superhelical twist. The first and last strands cross each other at an angle of about 90°, corresponding to the general canonical α/β fold (11, 16). Superposition of the EstE1 model structure with the crystal structure of AFEST (Protein Data Bank [PDB] code 1JJI) resulted in a root-mean-square deviation of 0.5 Å among 1,208 Cα atoms. The superposition of EstE1 and EST2 structures (PDB code 1EVQ) also displayed a good root-mean-square value of 1.1 Å among 980 Cα atoms. Secondary-structure-driven sequence alignment, using the ENDscript web server (8), between the predicted secondary structure of the final EstE1 model and the reference protein AFEST as well as EST2 showed that all share a high degree of similarity in both secondary structures and amino acid sequences (Fig. 2).

Previously, structural alignments and computer-aided statis-

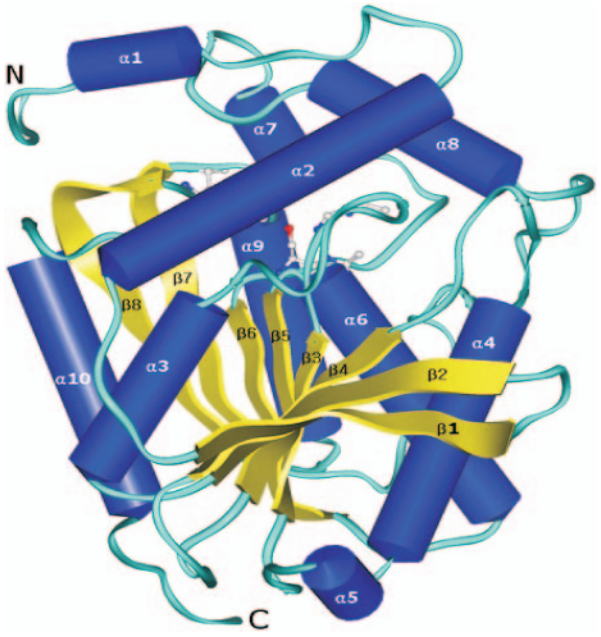

FIG. 1. 3D model of EstE1. Homology modeling of EstE1 was performed by using the Modeler program (18) in the InsightII software package (molecular modeling package, version 2000; Accelrys Inc., San Diego, CA). The hypothetical 3D model was then energy minimized using the Discover program in InsightII. Energy minimization was performed by the method of steepest descents until the energy gradient fell below 1.0 kcal/mol · Å, followed by application of the conjugate gradient minimization method until the energy gradient fell below 0.1 kcal/mol · Å. The model of EstE1 was verified by the Profile 3D (13) and PROCHECK (12) programs. The final model structure has been deposited in the PDB with accession number 2bzq. The α-helical segments are shown in blue and labeled sequentially as α1 to α10. β-Sheets are shown in yellow and labeled β1 to β8. The catalytic triad residues are shown in ball-and-stick representation. N and C denote the N and C termini, respectively.

* Corresponding author. Mailing address: Department of Biotechnology, Yonsei University, 134 Shinchon-dong, Seodaemun-gu, Seoul 120-749, South Korea. Phone: (822) 2123-2881. Fax: (822) 362-7265. E-mail: jwoh@yonsei.ac.kr.

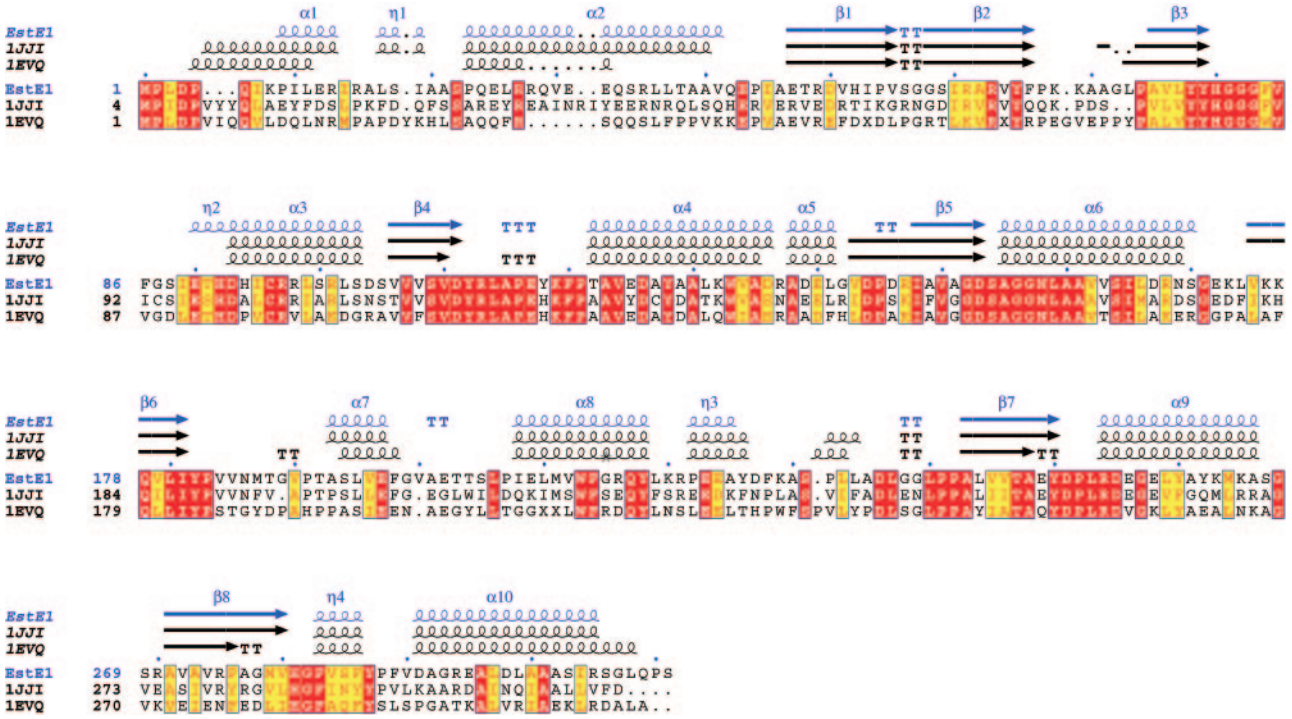

FIG. 2. Alignment of secondary structures of thermostable esterases in the HSL family. The homology-modeled structure of EstE1 (PDB 2bzq), along with the known structures of AFEST (PDB 1JJI) and EST2 (PDB 1EVQ), was used for structure and sequence alignment using ENDscript. Secondary structures are shown above the alignment: helices with squiggles, β strands with arrows, turns with TT letters, and 3_{10}-helices with η letters. Identical residues and residues with similar properties are shown in white on a red background and in red on a yellow background, respectively.

tical analyses of representative members of the HSL family esterase/lipase identified putative family-specific amino acid replacement patterns in the mesophilic-thermophilic direction of Gln replacing Arg, Gly replacing Ala, Gly replacing Arg, Ser replacing Ala, Thr replacing Arg, and Asp replacing Glu (1, 14). By comparison of the sequences and 3D protein structures, we identified the above-described amino acid changes as follows in the order of BFAE/EstE1/AFEST/EST2: Thr103/Arg61/Arg68/Lys62, Gly108/Ala75/Val81/Ala76, Thr132/Arg97/Arg103/Arg98, Gly161/Ala123/Ala129/Ala124, Gly183/Arg147/Lys153/Arg148, and Gly191/Ala155/Ala161/Ala156. We focused on the four residues Arg61, Ala75, Arg97, and Arg147. The counterpart residues of EstE1 Arg97 and Arg147, which form an ion pair network, were previously identified as important for the thermostability of EST2 (14) and thus were chosen to verify the predicted structure of EstE1. Ala61 was selected for mutagenesis analysis to demonstrate that a further extended ion pair network is involved in the thermostability of

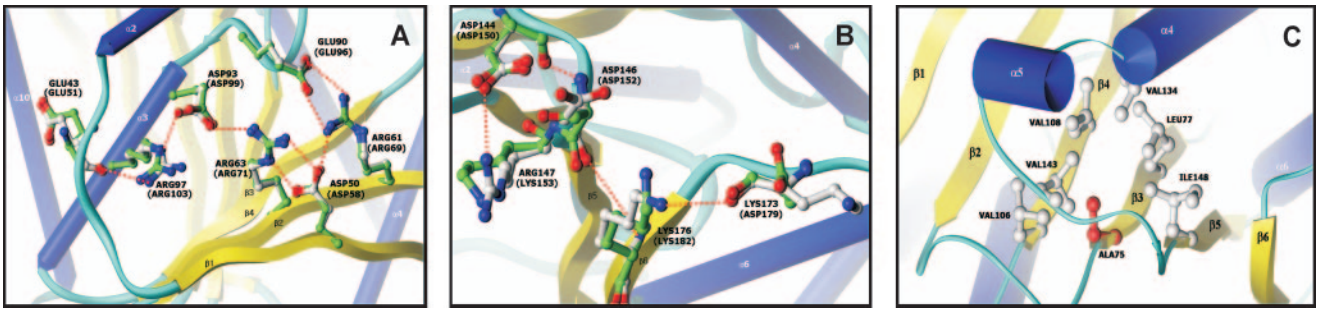

FIG. 3. Thermostability determinants of EstE1. Details of the ion pair network formed by Arg61 and Arg97 (A) and Arg147 (B). The ion pair network around Arg97 in EstE1 stabilizes the EstE1 structure through interactions among the α3-helix, the β1- and β2-sheets, and the two loops between the α2-helix and the β1-sheet and between the α3-helix and the β3-sheet. The ion pair network around Arg147 stabilizes the two nearby β-sheets β5 and β6. Hydrogen bonds calculated with a maximum distance of 4 Å are shown by red dots. AFEST sequence numbers are shown in parentheses below the EstE1 sequence. The ion pair networks observed around Arg61, Arg97, and Arg147 of EstE1 are also conserved in AFEST. (C) Interaction of Ala75 with surrounding residues in the EstE1 3D model. Ala75 and other interacting residues are shown in red and white, respectively. Surrounding hydrophobic residues were selected by searching a maximum distance of 5 Å from Ala75. Ala75 fits well into the cavity generated by the surrounding hydrophobic residues Leu77 (β3), Val106 (β4), Val108 (β4), Val134 (α4), Val143 (between α5 and β5), and Ile148 (β5).

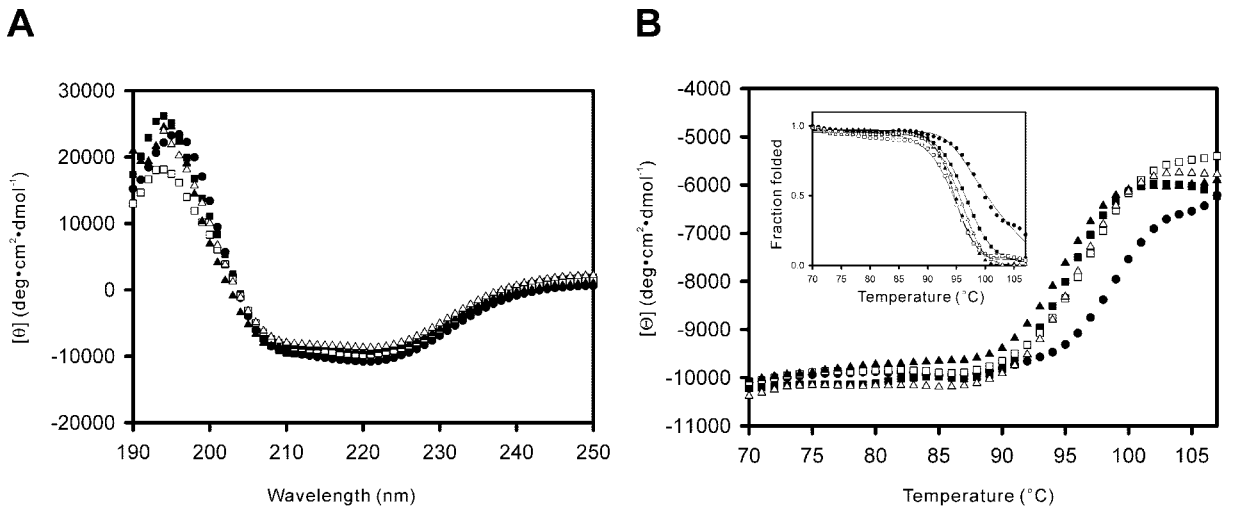

FIG. 4. Structure-thermostability relationship in EstE1. (A) Far-UV CD spectra of wild-type EstE1 (●), $EstE1_{R61A}$ (■), $EstE1_{A75G}$ (□), $EstE1_{R97A}$ (▲), and $EstE1_{R147A}$ (△). The EstE1 esterase gene (17) was PCR amplified and cloned into the expression vector pET-22b(+) (Novagen). Mutants of EstE1 were constructed by site-directed mutagenesis using the overlap extension method with PCR (10). Protein expression and purification were performed as previously described for wild-type EstE1 (17) with slight modifications. Cell lysates obtained by sonication in 10 ml of binding buffer A (50 mM Na-phosphate [pH 8.0], 300 mM NaCl, 10 mM imidazole, 10 mM β-mercaptoethanol, and 10% glycerol) were applied, without heat treatment, to Ni-nitrilotriacetic acid-agarose resin (QIAGEN). CD spectra were collected on a J-810 spectropolarimeter (Jasco, Tokyo, Japan) equipped with a Peltier temperature control system (model PTC-423S). All measurements were performed with purified esterase samples (0.2 mg/ml) in 10 mM potassium phosphate buffer (pH 7.0). Samples were scanned five times with a bandwidth of 1 nm and a response time of 1 s from 190 to 250 nm at a rate of 100 nm/min. Plots of molar ellipticity versus wavelength in far-UV range of wild-type EstE1 and its mutant are nearly superimposable. (B) Thermal denaturation profiles for wild-type EstE1, $EstE1_{R61A}$, $EstE1_{A75G}$, $EstE1_{R97A}$, and $EstE1_{R147A}$. Changes in molar ellipticity at 222 nm at a scan rate of 1°C/min in the temperature range of 70 to 110°C were measured, and the fractions folded are plotted. Because of irreversible unfolding of EstE1 proteins under these CD spectroscopy conditions, T_{app} values ($N = N_o/2$ but not necessarily $N = U = 1/2$ as obtained from a reversible two-state unfolding process in equilibrium) were estimated by fitting the data using the five-parameter sigmoid function from the curve-fitting program SIGMAPLOT, followed by determining the inflection point by numerical differentiation of the curves with MATLAB 7.0.4. For all EstE1 proteins, the decrease of the fraction folded was assumed to be proportional to the CD signal with rising temperatures.

EstE1. Mandrich et al. (14) proposed, without experimental evidence, the possible effect of hydrophobic interactions at EST2 Ala76 and AFEST Val81 on the thermostability of these esterases. Our detailed inspection of the EstE1 counterpart Ala75 in the EstE1 3D model showed that Ala75 is probably involved in filling the cavity formed by the α4, α5, β3, β4, and β5 regions of EstE1 (Fig. 3). This hydrophobic core cavity in the central β-sheet is also observed in both

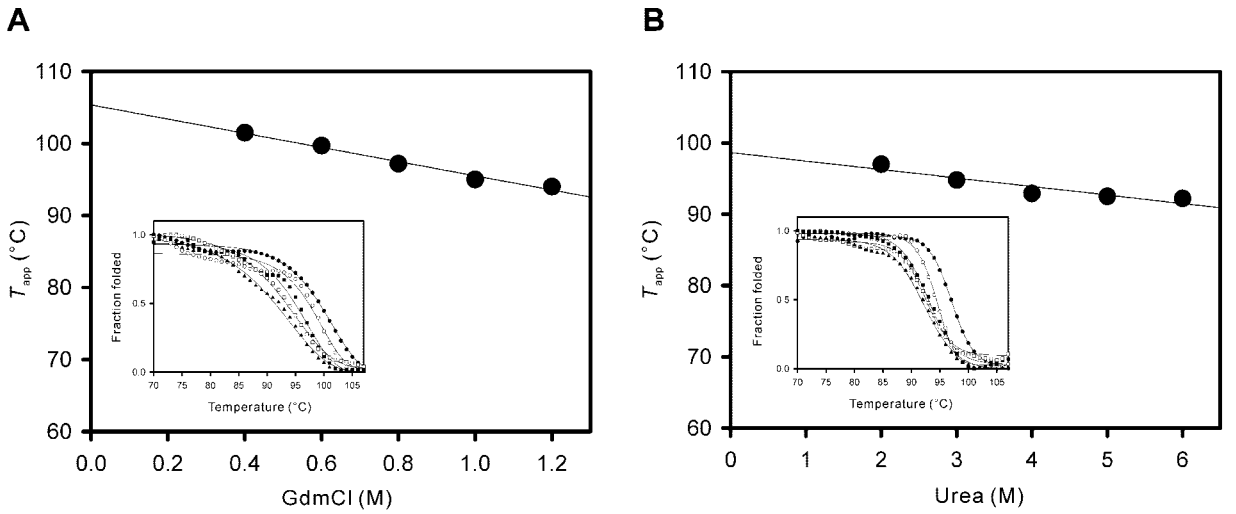

FIG. 5. Thermal denaturation profiles of EstE1 in the presence of denaturants. T_{app} values measured at various concentrations of guanidium chloride (GdmCl) (A) and urea (B) were plotted to estimate the T_{app} value in the absence of the denaturants by linear extrapolation. Shown in the inset of panel A are the temperature-induced denaturation curves for EstE1 in the presence of 0.4 M (●), 0.6 M (○), 0.8 M (■), 1.0 M (□), and 1.2 M (▲) guanidium chloride. Shown in the inset of panel B are the temperature-induced denaturation curves of EstE1 in the presence of 2.0 M (●), 3.0 M (○), 4.0 M (■), 5.0 M (□), and 6.0 M (▲) urea.

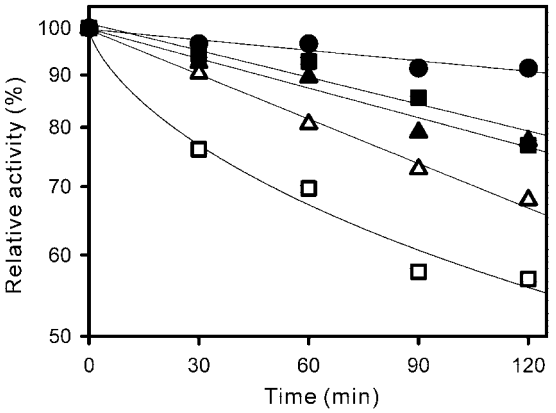

FIG. 6. Kinetic analysis of thermal stabilities of wild-type and mutant EstE1. The enzymes (6.0 μM) wild-type EstE1 (●), $EstE1_{R61A}$ (■), $EstE1_{A75G}$ (□), $EstE1_{R97A}$ (▲), and $EstE1_{R147A}$ (△) in 20 mM potassium phosphate buffer (pH 7.0) were incubated at 95°C for the indicated times. Residual activities were then determined by measuring the amount of *p*-nitrophenol released by esterase-catalyzed hydrolysis as described previously (17). The activity of a nonincubated sample was defined as 100%.

AFEST and EST2 and was occupied by similarly conserved hydrophobic residues. Comparison of amino acid environments in this hydrophobic core cavity showed that Ala75 in EstE1 and its counterparts Val81 in AFEST and Ala76 in EST2 have Gly108 in BFAE as a mesophilic counterpart. This analysis indicates that the volume of amino acids might be the key factor that determines their ability to fill the cavity in the central β-sheet. Ala and Val adequately fit within this cavity, while Gly is too small. Such tight packing of hydrophobic protein cores has been considered one of the major stabilizing factors for thermophiles (3, 4, 9).

To verify the role of the amino acid residues descried above in the thermostability of EstE1, we expressed and purified wild-type EstE1 and its mutants with a single amino acid substitution at the above-mentioned four positions. Circular dichroism (CD) spectra of the four purified mutants of EstE1 in the far-UV region at 20°C were very similar to the spectrum of wild-type EstE1 (Fig. 4A), indicating that the integrity of the secondary structure of these proteins was not affected by the introduction of mutations. We then measured the apparent transition temperatures (T_{app}) as described previously (7) to compare thermostabilities of EstE1 proteins. The T_{app} values for the $EstE1_{R61A}$, $EstE1_{A75G}$, $EstE1_{R97A}$, and $EstE1_{R147A}$ mutants were estimated to be 96.7°C, 94.6°C, 95.5°C, and 95.9°C, respectively. The T_{app} value of wild-type EstE1 had to be estimated by measuring the molar ellipticity at 222 nm in the presence of denaturant, because its CD spectra showed an insufficient posttransitional baseline. The T_{app} value at zero denaturant, which was obtained by extrapolation (Fig. 5A [for guanidium chloride] and B [for urea]), was in the range of 99 to 105°C. Furthermore, wild-type EstE1 lost only 9% of initial activity after incubation at 95°C for 120 min, whereas decreases of approximately 24, 46, 23, and 33% of initial activities were observed for $EstE1_{R61A}$, $EstE1_{A75G}$, $EstE1_{R97A}$, and $EstE1_{R147A}$, respectively (Fig. 6). These results are in agreement with the thermal denaturation experiment results. Of note is that a change in the Ala75 residue that is believed to have a stabilizing effect through tight packing in the hydrophobic core of EstE1 with its mesophilic counterpart Gly found in BFAE altered the thermostability of EstE1 more effectively than other mutations at the Arg61, Arg97, and Arg147 residues.

Thermostability of proteins is likely to be an outcome of various factors, including H-bond, ion pair network, hydrophobic interaction, disulfide bonding, metal coordination, and protein oligomerization (15, 19). Our limited analysis of thermostabilization determinants using a predicted 3D model of EstE1 cannot rule out other critical residues that may contribute to the extremely high thermostability of EstE1. Nevertheless, our results provide a common basis for the rational engineering of esterases/lipases in the HSL family to increase thermostability through combination with other determinants. Furthermore, our mutational analysis of EstE1 verifies the homology-modeled EstE1 3D structure.

Protein structure accession number. The final model structure of EstE1 was deposited in the PDB with accession number 2bzq.

This work was supported by the Korea Research Foundation grant funded by the Korean Government (KRF-2004-C00148) and, in part, by the IMT 2000 grant funded by the Korea Ministry of Commerce, Industry, and Energy (IMT 2000-00016108).

REFERENCES

1. **Argos, P., M. G. Rossman, U. M. Grau, H. Zuber, G. Frank, and J. D. Tratschin.** 1979. Thermal stability and protein structure. Biochemistry **18:** 5698–5703.
2. **Bourne, P. C., M. N. Isupov, and J. A. Littlechild.** 2000. The atomic-resolution structure of a novel bacterial esterase. Structure **8:**143–151.
3. **Britton, K., P. Baker, K. Borges, P. Engel, A. Pasquo, D. Rice, F. Robb, R. Scandurra, T. Stillman, and K. Yip.** 1995. Insights into thermal stability from a comparison of the glutamate dehydrogenases from *Pyrococcus furiosus* and *Thermococcus litoralis.* Eur. J. Biochem. **229:**688–695.
4. **Chen, J., Z. Lu, J. Sakon, and W. E. Stites.** 2000. Increasing the thermostability of staphylococcal nuclease: implications for the origin of protein thermostability. J. Mol. Biol. **303:**125–130.
5. **De Simone, G., S. Galdiero, G. Manco, D. Lang, M. Rossi, and C. Pedone.** 2000. A snapshot of a transition state analogue of a novel thermophilic esterase belonging to the subfamily of mammalian hormone-sensitive lipase. J. Mol. Biol. **303:**761–771.
6. **De Simone, G., V. Menchise, G. Manco, L. Mandrich, N. Sorrentino, D. Lang, M. Rossi, and C. Pedone.** 2001. The crystal structure of a hyperthermophilic carboxylesterase from the archaeon *Archaeoglobus fulgidus.* J. Mol. Biol. **314:**507–518.
7. **Duy, C., and J. Fitter.** 2005. Thermostability of irreversible unfolding alpha-amylases analyzed by unfolding kinetics. J. Biol. Chem. **280:**37360–37365.
8. **Gouet, P., X. Robert, and E. Courcelle.** 2003. ESPript/ENDscript: extracting and rendering sequence and 3D information from atomic structures of proteins. Nucleic Acids Res. **31:**3320–3323.
9. **Haney, P., J. Konisky, K. K. Koretke, Z. Luthey-Schulten, and P. G. Wolynes.** 1997. Structural basis for thermostability and identification of potential active site residues for adenylate kinases from the archaeal genus *Methanococcus.* Proteins **28:**117–130.
10. **Ho, S. N., H. D. Hunt, R. M. Horton, J. K. Pullen, and L. R. Pease.** 1989. Site-directed mutagenesis by overlap extension using the polymerase chain reaction. Gene **77:**51–59.
11. **Holmquist, M.** 2000. Alpha/beta-hydrolase fold enzymes: structures, functions and mechanisms. Curr. Protein Pept. Sci. **1:**209–235.
12. **Laskowski, R. A., J. A. Rullmann, M. W. MacArthur, R. Kaptein, and J. M. Thornton.** 1996. AQUA and PROCHECK-NMR: programs for checking the quality of protein structures solved by NMR. J. Biomol. NMR **8:**477–486.
13. **Luthy, R., J. U. Bowie, and D. Eisenberg.** 1992. Assessment of protein models with three-dimensional profiles. Nature **356:**83–85.
14. **Mandrich, L., M. Pezzullo, P. Del Vecchio, G. Barone, M. Rossi, and G. Manco.** 2004. Analysis of thermal adaptation in the HSL enzyme family. J.

Mol. Biol. **335:**357–369.
15. **Nordberg Karlsson, E., S. J. Crennell, C. Higgins, S. Nawaz, L. Yeoh, D. W. Hough, and M. J. Danson.** 2003. Citrate synthase from *Thermus aquaticus*: a thermostable bacterial enzyme with a five-membered inter-subunit ionic network. Extremophiles **7:**9–16.
16. **Ollis, D. L., E. Cheah, M. Cygler, B. Dijkstra, F. Frolow, S. M. Franken, M. Harel, S. J. Remington, I. Silman, J. Schrag, et al.** 1992. The alpha/beta hydrolase fold. Protein Eng. **5:**197–211.
17. **Rhee, J.-K., D.-G. Ahn, Y.-G. Kim, and J.-W. Oh.** 2005. New thermophilic and thermostable esterase with sequence similarity to the hormone-sensitive lipase family, cloned from a metagenomic library. Appl. Environ. Microbiol. **71:**817–825.
18. **Sali, A., and T. L. Blundell.** 1993. Comparative protein modelling by satisfaction of spatial restraints. J. Mol. Biol. **234:**779–815.
19. **Sterner, R., and W. Liebl.** 2001. Thermophilic adaptation of proteins. Crit. Rev. Biochem. Mol. Biol. **36:**39–106.
20. **Wei, Y., J. A. Contreras, P. Sheffield, T. Osterlund, U. Derewenda, R. E. Kneusel, U. Matern, C. Holm, and Z. S. Derewenda.** 1999. Crystal structure of brefeldin A esterase, a bacterial homolog of the mammalian hormone-sensitive lipase. Nat. Struct. Biol. **6:**340–345.